Available online at www.sciencedirect.com

ScienceDirect

IFAC Papers Online CONFERENCE PAPER ARCHIVE

IFAC-PapersOnLine 49-13 (2016) 093–098

Experimental Evaluation of Reset Control for Improved Stage Performance

M.F. Heertjes [*,**] **K.G.J. Gruntjens** [***] **S.J.L.M. van Loon** [**] **N. van de Wouw** [**,****,†] **W.P.M.H. Heemels** [**]

[*] *ASML, Mechatronic Systems Development, Veldhoven, The Netherlands and Eindhoven University of Technology, Mechanical Engineering, Eindhoven, The Netherlands. (marcel.heertjes@asml.com)*

[**] *Eindhoven University of Technology, Mechanical Engineering, Eindhoven, The Netherlands.*

[***] *Océ Technologies, Mechanical Department, Venlo, The Netherlands.*

[****] *Department of Civil, Environmental and Geo-Engineering, University of Minnesota, Minneapolis, MN 55455 USA.*

[†] *Delft Center for Systems and Control, Delft University of Technology, Delft, The Netherlands.*

Abstract: A reset integral controller is discussed that induces improved low-frequency disturbance rejection properties under double integrator control without giving the unwanted increase of overshoot otherwise resulting from adding an extra linear integrator. To guarantee closed-loop stability, a (conditional) reset condition is used that restricts the input-output behavior of the dynamic reset element to a $[0, \alpha]$-sector with α a positive (finite) gain. As a result, stability can be guaranteed on the basis of a circle criterion-like argument and checked through (measured) frequency response data. Both stability and performance of the control design will be discussed via measurement results obtained from a wafer stage system of an industrial wafer scanner.

Keywords: Circle criterion, Lyapunov stability, motion systems, reset control, wafer scanners.

1. INTRODUCTION

This paper discusses a reset integral controller design to cope with the conventional trade-off between a) improved low-frequency disturbance suppression through integral control and b) desired transient response, which in view of the mentioned integral control usually deteriorates. This trade-off generically arises in high-precision motion control applications like for example wafer scanners, which are used in the production of chips, and which require nanometer accuracies under aggressive motion profiles; for the control of wafer scanners see also (Butler, 2011).

Nonlinear control has been opted by many researchers (Seron & Goodwin, 1996) in an attempt to balance the above-mentioned trade-off in a more desirable manner. An interesting concept in this regard is reset control, see for example the Clegg integrator that later developed into first-order reset elements (FORE), see Clegg (1958); Horowitz & Rosenbaum (1975); Zaccarian et al. (2005). The Clegg integrator is a simple integrator that resets its state to zero upon zero input crossings. Its describing function possesses a 20 dB/decade amplitude decay with 38.15 degrees of phase lag instead of the 90 degrees phase lag corresponding to a linear integrator (Clegg, 1958).

With these advantages in mind, recently a variable-gain integrator with reset properties has been proposed by Heertjes et al. (2015). In this work, the variable-gain integrator with reset combines a variable-gain integral controller with a Clegg integrator. The measurement results obtained for this type of controller applied to a piezo-actuated lens system clearly demonstrated its benefits. Stability of the closed-loop reset system essentially boils down to satisfying two conditions: i) a flow condition in the intervals between resets, and ii) a jump condition at the resets, see also Aangenent et al. (2010); Baños et al. (2011); Beker et al. (2004); Zaccarian et al. (2005, 2011); Carrasco et al. (2010). For the base-nonlinear system, i.e., the variable-gain integrator without the reset, stability has been guaranteed by the application of the positive real lemma, thereby guaranteeing satisfactory the flow condition. For the closed-loop nonlinear system with reset, a quadratic Lyapunov function candidate is found that satisfies both the flow and the jump condition. This is done by pursuing an LMI-(linear matrix inequalities) based approach. In the high-precision industry, however, using LMI-based design conditions is considered as less desirable, because it requires a parametric model of the plant to be controlled, which is often difficult to obtain and which rarely meets the requirements imposed on model accuracy. Moreover, LMI stability analysis only renders limited physical or controller tuning insights compared to frequency-domain techniques, while this is crucial in support of the development of a generically applicable controller strategy.

2405-8963
Peer review under responsibility of International Federation of Automatic Control.
10.1016/j.ifacol.2016.07.933

In this paper, inspired by Heertjes et al. (2015), a lag filter is used where the integrator is replaced by a Clegg integrator. The flow and jump sets are designed such that the input-output behavior of the reset element belongs to the sector $[0, \alpha]$ with $\alpha > 0$ a positive (finite) gain. Based on this insight, input-to-state stability of the closed-loop system with reset can be guaranteed by combining a circle criterion-like argument (Arcak et al., 2003) together with a detectability condition for the reset element; note that the latter includes an integrator, which is not memoryless, and thus requires extra attention beyond the conventional circle criterion argument. The above stability conditions can be assessed by evaluating (measured) frequency response data of the linear part of the closed-loop system in relation to the gain α. The main contributions of the paper are the application of this reset control to the wafer stage of an industrial wafer scanner and the demonstration of the frequency-domain design in practice.

The remainder of this paper is organized as follows. In Section 2, the reset control design is discussed in more detail. This includes a circle criterion-like stability argument that results in easy-to-check stability conditions. In Section 3, measurement results are discussed that are obtained by application of the reset controller to a wafer stage system. Section 4 summarizes the main conclusions.

2. RESET CONTROL DESIGN

Consider the reset control system in Fig. 1 where the nonlinear element, i.e., the reset integrator, captured in $\mathcal{R}$ is being isolated from the linear dynamics represented by $\mathcal{H}$. In the figure, r represents a reference to be tracked,

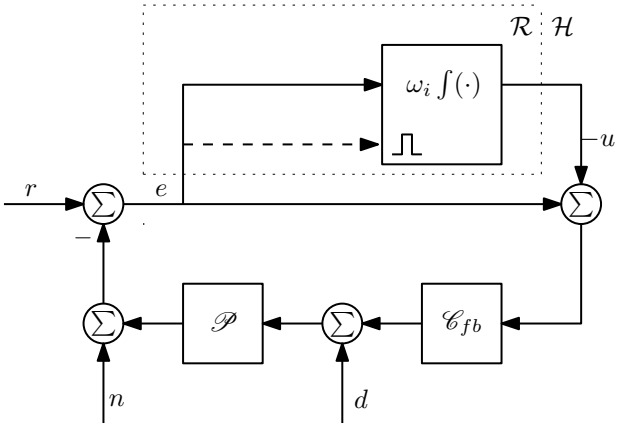

Fig. 1. Simplified schematics of a reset control system.

e is a closed-loop error signal, $\mathscr{C}_{fb}$ a nominal (linear) PID-based feedback controller, d a force disturbance, $\mathscr{P}$ the plant, n the output disturbance (e.g., sensor noise), and $-u$ the output of the reset integrator. For the ease of presentation, it should be mentioned that feedforward control, which does not affect the upcoming closed-loop stability analysis, has been omitted from the figure. However, all measurement results presented later on will include the effect of a mass/snap feedforward controller with delay compensation (having the motion control setting in mind).

To obtain stability conditions that allow for verification on the basis of frequency response data, the system in Fig. 1 is transformed to a Lur'e-type system, see Fig. 2. Note that the essential difference with a true Lur'e system lies in the fact that a *dynamical* nonlinear system $\mathcal{R}$ — $\mathcal{R}$ contains an integrator — is considered rather than a memoryless (and static) nonlinearity. In Zaccarian et al. (2005) it is

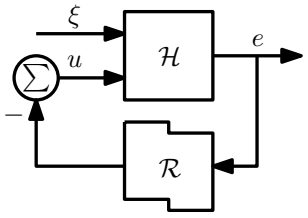

Fig. 2. Lur'e-type system representation.

remarked that a classical Clegg integrator (with input e and output $-u$) is characterized by the property that input and output can never have opposite signs. This particular property has been exploited in, e.g. Zaccarian et al. (2005), Nešić et al. (2008), and Aangenent et al. (2010), where the integrator resets whenever $eu \leq 0$. From the frequency-domain perspective such as pursued in this paper, this reset condition can be viewed as the input-output pair $(e, -u)$ corresponding to the sector $[0, \infty]$. Application of the (frequency-domain) circle criterion would then require $\mathcal{H}$ to be positive real, a feature that is rarely met in motion control applications. We therefore propose to choose the reset condition of the switching integral controller with reset such that the input-output pair $(e, -u)$ corresponds to the sector $[0, \alpha]$ with $\alpha \in \mathbb{R}_{>0}$ being constant. In the case of $\mathcal{R}$ being a static memoryless element, input-to-state stability of the closed-loop system as shown in Fig. 2 can be simply proved by evaluating the circle criterion. However, since $\mathcal{R}$ contains dynamical elements (in this case an integrator) additional arguments are needed to ensure internal stability of $\mathcal{R}$, and consequently ISS of the reset control system in Fig. 2 including this integrator state.

2.1 Closed-Loop Model Representation

Consider Fig. 2 where $\mathcal{H}$ represents a continuous-time LTI dynamical system that in state-space description reads

$$\mathcal{H} : \begin{cases} \dot{x}_h(t) &= Ax_h(t) + Bu(t) + B_\xi \xi(t) \\ e(t) &= Cx_h(t) + D_\xi \xi(t) \end{cases}, \qquad (1)$$

with $e(t), u(t) \in \mathbb{R}$, and $x_h(t) \in \mathbb{R}^{n_h}$ the state vector containing the (physical) states of plant $\mathscr{P}$ and feedback controller $\mathscr{C}_{fb}$ in Fig. 1 at time $t \in \mathbb{R}_{\geq 0}$. Moreover, $\xi(t) = [r(t)\ d(t)\ n(t)]^T \in \mathbb{R}^{3\times 1}$ denotes the augmented exogenous input vector, and (A, B, C) is assumed to correspond to a minimal realization. The transfer function between input $u(s)$ and output $e(s)$ of (1) is the complementary sensitivity function $\mathscr{S}_{ch}(s)$, which is given by

$$\begin{aligned} \mathscr{S}_{ch}(s) &:= C(sI - A)^{-1}B \\ &= \frac{\mathscr{P}(s)\mathscr{C}_{fb}(s)}{1 + \mathscr{P}(s)\mathscr{C}_{fb}(s)}. \end{aligned} \qquad (2)$$

Consider the nonlinear dynamical system $\mathcal{R}$ with input-output pair $(e, -u)$ which consists of the reset integrator and which is given by the following impulsive differential equation (IDE)

$$\mathcal{R} : \begin{cases} \dot{x}_i(t) &= \omega_i e(t), & \text{if } (e, -u) \in \mathcal{F}, \\ x_i(t^+) &= 0, & \text{if } (e, -u) \in \mathcal{J}, \\ -u(t) &= x_i(t). \end{cases} \qquad (3)$$

Note that the reset condition is defined in terms of a flow set $\mathcal{F}$ and a jump set $\mathcal{J}$. As such, system $\mathcal{R}$ behaves continuously conform the differential equation in (3) as long as $(e,-u)\in\mathcal{F}$ whereas state x_i will jump instantaneously from x_i to $x_i^+=0$ when $(e,-u)\in\mathcal{J}$. Now define the flow set $\mathcal{F}$ and the jump set $\mathcal{J}$ according to

$$\begin{aligned}\mathcal{F}&=\{(e,-u)\in\mathbb{R}\mid eu\leq-\frac{1}{\alpha}u^2\}\\ \mathcal{J}&=\{(e,-u)\in\mathbb{R}\mid eu\geq-\frac{1}{\alpha}u^2\},\end{aligned}\tag{4}$$

with $\alpha\in\mathbb{R}_{>0}$. Given (3) and (4), the input-output pair $(e,-u)$ of (3) is (apart from a possible initial condition) restricted to the sector $[0,\ \alpha]$ as illustrated by Fig. 3.

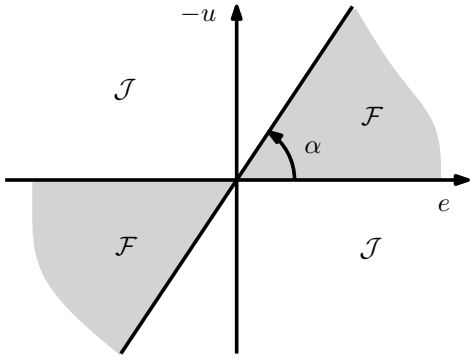

Fig. 3. Graphical representation of the flow set $\mathcal{F}$ and the jump set $\mathcal{J}$ as defined by (4).

Remark 1. The sets $\mathcal{F}$ and $\mathcal{J}$ can be defined in various ways, although, one must be cautious to avoid Zeno behavior, beating, and deadlock. Deadlock, beating, and Zeno behavior can often be avoided by time-regularization (see for example Nešić et al. (2008) or Forni et al. (2011)), i.e. after every reset instant, x_i evolves according to the continuous dynamics in (3) for some finite time interval. Time regularization occurs quite naturally in most practical implementations that involve a sampled-data implementation of the controller, such as in the experimental setting investigated in Section 3. As such, deadlock, beating, and Zeno behavior are disregarded in this paper and it is assumed that solutions to the closed-loop system are well-defined for all $t\in\mathbb{R}_{\geq0}$.

2.2 Closed-loop Stability

Consider the closed-loop system in Fig. 2 with the corresponding state vector $x(t):=[x_i(t)\ x_h^T(t)]^T\in\mathbb{R}^n$ at time $t\in\mathbb{R}_{\geq0}$ in which $x_i(t)\in\mathbb{R}$ is governed by (3) and $x_h(t)\in\mathbb{R}^{n_h}$ consists of both the states of plant $\mathscr{P}$ as well as the states of the controller $\mathscr{C}_{fb}$. System (1), (3), (4) is said to be input-to-state stable (ISS) with respect to input ξ if for any initial condition $x_0\in\mathbb{R}^n$ and any bounded input signal ξ, all solutions x satisfy

$$||x(t)||\leq\beta(||x_0||,t)+\gamma(||\xi_{[0,t]}||_\infty),\ \text{for all } t\in\mathbb{R}_{\geq0},\tag{5}$$

with β and γ being class $\mathcal{KL}$ and class $\mathcal{K}$ functions, respectively. As a result, the effect of the initial conditions (for zero input $r=n=v=0$) eventually fades away. For non-zero input, multiple steady-state solutions may occur within the compact (and invariant) set which is characterized by γ.

The following result poses sufficient conditions under which ISS of the closed-loop system (1), (3), (4) in Fig. 2 can be guaranteed; a detailed proof can be found in Van Loon et al. (2016).

Theorem 1. Consider the closed-loop system in Fig. 2 with $\mathcal{H}$ as in (1) and $\mathcal{R}$ as in (3), (4). Suppose there exists a constant $\alpha\in(0,\ \infty)$ satisfying the following conditions on the frequency response function $\mathscr{S}_{ch}(j\omega)$ given in (2):

$$\begin{aligned}&a)\quad \mathscr{S}_{ch}(j\omega)\text{ is Hurwitz,}\\ &b)\quad 1+\alpha\mathscr{S}_{ch}(j\infty)>0,\\ &c)\quad Re\{\mathscr{S}_{ch}(j\omega)\}>-\frac{1}{\alpha},\ \text{for all }\omega\in\mathbb{R}.\end{aligned}\tag{6}$$

Then the closed-loop system (1), (3), (4) in Fig. 2 is input-to-state stable (ISS) with respect to inputs ξ.

Sketch of Proof: A smooth function $W:\mathbb{R}^{n_h+1}\to\mathbb{R}$ is an ISS-Lyapunov function (ISSLF) for the system (1) with (3) and (4), if it satisfies, for $\kappa_i>0$, $i\in\{1,2,3,4\}$, the following conditions

$$\kappa_1\|x\|^2\leq W(x)\leq\kappa_2\|x\|^2,\tag{7a}$$

$$\dot{W}(x)\leq-\kappa_3\|x\|^2+\kappa_4\|w\|^2,\quad\text{for all } x\in\mathcal{F},\tag{7b}$$

$$W(x^+)\leq W(x),\quad\text{for all } x\in\mathcal{J}.\tag{7c}$$

The existence of an ISSLF guarantees ISS under the assumption that solutions are well-defined for all $t\in\mathbb{R}_{\geq0}$. In the remainder of the proof, the existence of such a function W is concisely demonstrated (under the hypotheses of the theorem) by the following four steps:

(1) disregard the internal (nonlinear) dynamics of $\mathcal{R}$ and exploit the fact that the input/output pairs $(e,-u)$ of $\mathcal{R}$ satisfy the sector condition $eu\leq-u^2/\alpha$ by the grace of the form of $\mathcal{F}$ and $\mathcal{J}$ in (4); introduce the following auxiliary system (called base-linear system)

$$\Sigma_{bls}:\begin{cases}\mathcal{H}:\begin{cases}\dot{x}_h=Ax_h+Bu+B_\xi\xi\\ e=Cx_h+D_\xi\xi\end{cases}\\ u=-\varphi(e),\end{cases}\tag{8}$$

in which $\varphi(e)$ satisfies the following sector condition

$$0\leq\varphi(e)\leq\alpha e,\tag{9}$$

for all $e\in\mathbb{R}$; the circle criterion is used to prove that the system Σ_{bls} admits a quadratic ISSLF $V:\mathbb{R}^{n_h}\to\mathbb{R}$;

(2) use a detectability condition on the state of $\mathcal{R}$ to construct a Lyapunov-like function $V_r:\mathbb{R}\to\mathbb{R}$ for the system $\mathcal{R}$ during flow, i.e., for $(e,-u)\in\mathcal{F}$;

(3) show that the resulting V of Step 1 and V_r of Step 2 can be combined into a function $W:\mathbb{R}^{n_h+1}\to\mathbb{R}$ that satisfies the ISSLF condition during flow of said function, i.e., (7b), for all $x\in\mathcal{F}$ of the total system combining $\mathcal{H}$ and $\mathcal{R}$;

(4) show that the ISSLF constructed in Step 3 does not increase during resets, thereby also satisfying the ISSLF condition during jumps, i.e., (7c), for all $x\in\mathcal{J}$; combining the results of Step 3 and Step 4 allows to construct a bound on the norm of the complete state as in (5).

The proof further consists of showing that there exists a smooth ISSLF $W:\mathbb{R}^{n_h+1}\to\mathbb{R}$ for the system defined by (1), (3), and (4) that is ISS according to (5); the full proof can be found in Van Loon et al. (2016). □

3. CASE STUDY: WAFER STAGE SYSTEM

In order to study the effectiveness of the reset control design, consider the example of a wafer scanner, see Fig. 4 for an artist impression of such a system. Most wafer scanners

Fig. 4. Artist impression of a wafer scanner.

exploit the lithographic principle in which ultraviolet light from a reticle or so-called mask is projected — through a lens system — onto the light-sensitive layers of a wafer. In this process, both reticle and wafer are supported by separate motion control systems being the reticle and the wafer stage system, respectively, that conduct a series of point-to-point motions, thereby allowing for different field exposures. Exposure of a field takes place while scanning, i.e., the wafer stage chuck moves with constant velocity (and with nanometer precision) under a lens system. As soon as one field exposure is finished, the wafer stage chuck moves toward the next field. Roughly speaking, a single wafer contains about 100 fields. As to minimize time between two subsequent exposures, and thus enhance throughput, positioning between fields is done with aggressive motion profiles having acceleration levels in the order of 50 $\mathrm{m}\cdot\mathrm{s}^{-2}$. In the remainder of the case study, we particularly focus on the control of the wafer stage system.

The wafer stage system often exploits a dual-stroke principle in which a long-stroke is used for coarse positioning with micrometer accuracy while a short-stroke is used for fine-positioning with nanometer accuracy. Consider the short-stroke control design in scanning y-direction for which the open-loop characteristics are depicted in Fig. 5. Based on measured frequency response function data, firstly the figure shows the characteristics of $\mathscr{L}(j\omega) = \mathscr{C}_{fb}(j\omega)\mathscr{P}(j\omega)$ in grey, i.e., the default control design from Fig. 1, having a bandwidth of 259.6 Hz with a phase margin of 19.9 degrees and a gain margin of 4.1 dB. Secondly, the figure shows the estimated characteristics for the reset control design in red, which are based on a describing function analysis, and given by

$$\mathscr{L}_{reset}(j\omega) = \mathscr{L}(j\omega)\cdot\left(1+\frac{\omega_i}{j\omega}\left(1+\frac{4j}{\pi}\right)\right), \qquad (10)$$

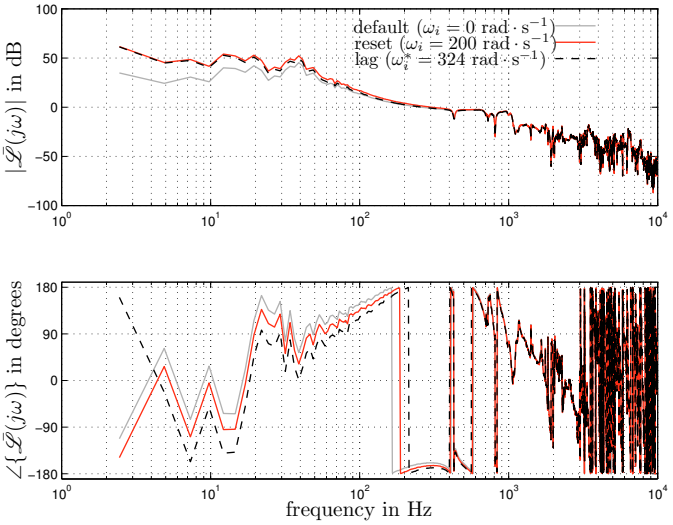

Fig. 5. Open-loop characteristics $\bar{\mathscr{L}} \in \{\mathscr{L}, \mathscr{L}_{reset}, \mathscr{L}_{lag}\}$ based on measurement data with (red) or without (grey) extra reset integrator or with (dashed black) an extra integrator ($\omega_i^* = 1.62\omega_i$) but without having reset functionality.

see also Heertjes et al. (2015). The latter clearly shows the additional low-frequency gain induced by the extra reset integrator, but with less phase lag otherwise induced when introducing an extra linear integrator, or

$$\mathscr{L}_{lag}(j\omega) = \mathscr{L}(j\omega)\cdot\left(1+\frac{\omega_i^*}{j\omega}\right), \qquad (11)$$

with $\omega_i^* = 1.62\omega_i$ scaled with $|1+4j/\pi|$ as to obtain equal low-frequency gain, i.e., the extra integrator in Fig. 1 without reset functionality (indicated in dashed black). For $\omega_i = 200$ rad $\cdot\, s^{-1}$, $\mathscr{L}_{reset}$ from (10) demonstrates a bandwidth of 302.8 Hz along with a phase margin of 15.6 degrees and a gain margin of 2.9 dB. Thirdly, Fig. 5 shows the characteristics obtained by removing the reset functionality, giving $\mathscr{L}_{lag}$ from (11). This leads to a bandwidth of 263.3 Hz with a phase margin of 9.1 degrees and a gain margin of 3.2 dB. Hence by application of Nyquist' Theorem, it can be concluded that the linear designs $\mathscr{L}$ and $\mathscr{L}_{lag}$ render a robustly stable closed-loop system. For the reset control system, in general, no conclusions regarding closed-loop stability can be drawn on the sole basis of $\mathscr{L}_{reset}$.

To guarantee closed-loop stability of the reset control system, consider Theorem 1. Note that conditions a) and b) are satisfied for the given choice of $\mathscr{L}$. A graphical representation of condition c) is shown in Fig. 6. From this figure (grey curve), it is clear that condition c) is satisfied for positive $\alpha \leq 1/2.38 \approx 0.4$, which (in practice) may be too small to render the reset control design effective; to fully exploit the Clegg integrator it is typically desirable to have $\alpha \gg 0.4$. To increase the value of α, a (notch) filter $\mathscr{N}$ can be applied to the output $-u$ in Fig. 1 while leaving the low-frequency signal intact; note that the introduction of such a filter $\mathscr{N}$ generally does not affect the outcome of the conditions a) and b) that were satisfied for the given choice of $\mathscr{L}$. The effect is shown by the red curve, which requires the evaluation of $\mathscr{S}_{ch}^*(j\omega) = \mathscr{N}(j\omega)\mathscr{S}_{ch}(j\omega)$ in condition c) and which is satisfied for positive $\alpha \leq 1/0.45 \approx 2.2$.

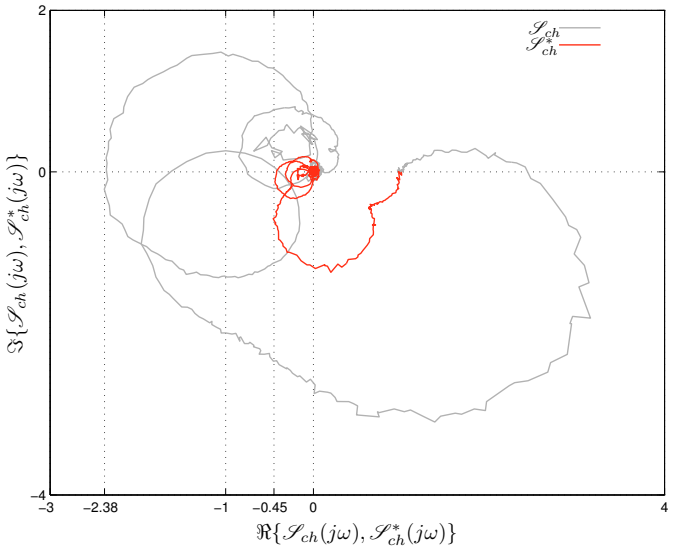

Fig. 6. Evaluation of condition c) from *Theorem 1* with measurement data either with (red) or without (grey) extra notch filter in $\mathscr{S}^*_{ch}(j\omega) = \mathscr{N}(j\omega)\mathscr{S}_{ch}(j\omega)$.

Having sufficient conditions to guarantee closed-loop stability, closed-loop performance can be studied using sensitivity analysis. Based on the (measured) open-loop frequency response functions from Fig. 5 and transfer reconstruction using describing functions, Fig. 7 shows the sensitivity function of the default control design (grey), the reset control design (red) using the describing function in (10), and the double integrator design (dashed black) obtained with the lag filter design in (11). It can be seen that the reset control design has extra (low-frequency) disturbance suppression properties compared to the default control design, which result from the extra integrator, but which induce hardly any significant high-frequency deterioration. The phase advantages associated with the reset clearly show when considering the lag filter design that resembles the reset control design apart from the reset, i.e., the design based on (10) compared with the design based on (11). Without reset, less suppression is obtained between 20 and 200 Hz whereas more amplification results around the bandwidth frequency of 260 Hz.

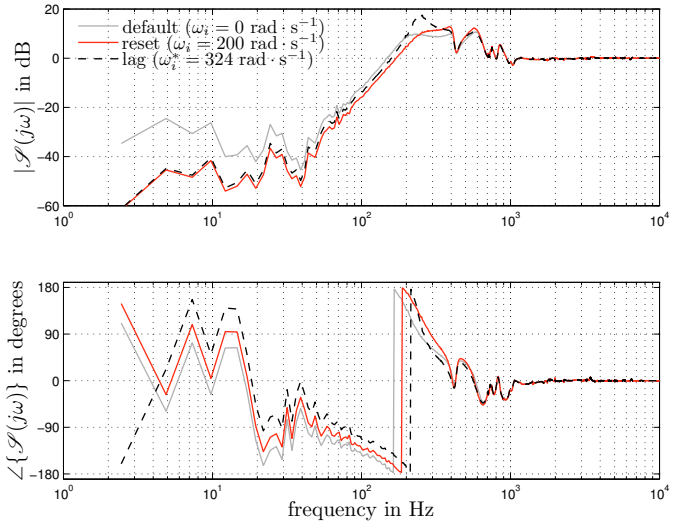

Fig. 7. Sensitivity magnitude plots based on measurement data with (red) or without (grey) extra reset integrator or with (dashed black) an extra integrator ($\omega_i^* = 1.62\omega_i$) but without having reset functionality.

In time-domain, measurement results are shown in Fig. 8. For four equal scanning motions — the dashed black curve represents the scaled acceleration profile — either with (red) or without (grey) extra reset integrator, it can be seen that extra disturbance suppression is obtained without the unwanted effect of extra overshoot and settling time. Note that there is not much room to improve upon state-of-the-art performance obtained with the default controller. Nevertheless, a significant performance improvement is demonstrated. This can be seen by filtering the error signal e either with a moving average filter ($\mathcal{M}_a$) or a moving standard deviation filter ($\mathcal{M}_{sd}$), or

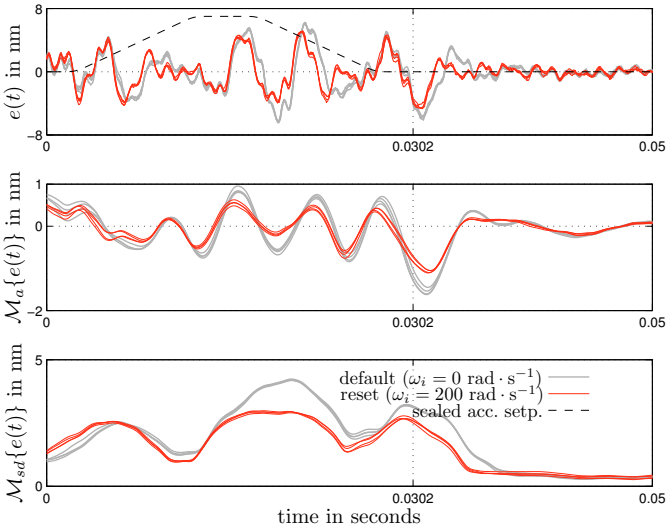

Fig. 8. Time series measurement: data of four responses to the same commanded reference (dashed) either with (red) or without (grey) extra reset integrator.

$$\mathcal{M}_a\{e(t)\} = \frac{1}{\eta}\int_{t-\frac{\eta}{2}}^{t+\frac{\eta}{2}} e(\tau)d\tau$$
$$\mathcal{M}_{sd}\{e(t)\} = \sqrt{\frac{1}{\eta}\int_{t-\frac{\eta}{2}}^{t+\frac{\eta}{2}} (e(\tau) - \mathcal{M}_a\{e(t)\})^2 d\tau}, \quad (12)$$

with $\eta \approx 2.57 \cdot 10^{-3}$ s a process window, $\mathcal{M}_a$ being a measure for on-product overlay, and $\mathcal{M}_{sd}$ being a measure for imaging. The result in Fig. 8 shows that from the start of exposure at $t = 0.0302$ seconds, $\|\mathcal{M}_a\{e\}\|_\infty$ decreases from 1.6 nanometer to 1.1 nanometer and $\|\mathcal{M}_{sd}\{e\}\|_\infty$ decreases from 3.1 nanometer to 2.6 nanometer. Hence, both signal norms are reduced with 0.5 nanometer, which is a significant reduction for this application.

Remark 2. It is important to mention that the results in Fig. 8 were obtained with $\alpha = 10$ (further increase of α did not have much effect on improved performance) and without using an extra notch filter $\mathscr{N}$ in the evaluation of $\mathscr{S}^*_{ch}(j\omega) = \mathscr{N}(j\omega)\mathscr{S}_{ch}(j\omega)$ in condition c). The circle criterion evaluation for the industrial wafer stage case guarantees stability for values of $\alpha \leq 0.4$ that induce only

marginal performance improvement. So regardless the fact that a frequency-domain tool toward tuning and stability of reset control systems is obtained, the practical effectiveness of this tool toward the demonstrated value of $\alpha = 10$ needs to be improved. Firstly, because closed-loop stability based on the conditions of Theorem 1 in this case cannot be guaranteed according to Fig.6. Secondly, because increasing α gave no indication toward unstable closed-loop behavior whatsoever. Closed-loop unstable behavior was encountered when ω_i was increased from $\omega_i = 200$ rad$\cdot$s^{-1} toward $\omega_i = 600$ rad$\cdot$s^{-1}, which relates to $\mathscr{L}_{lag}$ no longer satisfying condition a) in Theorem 1, i.e., the base-linear system becoming unstable.

In terms of frequency content, Fig. 9 shows both a power spectral density analysis (upper part) and a cumulative root-mean-square representation (lower part). It can be

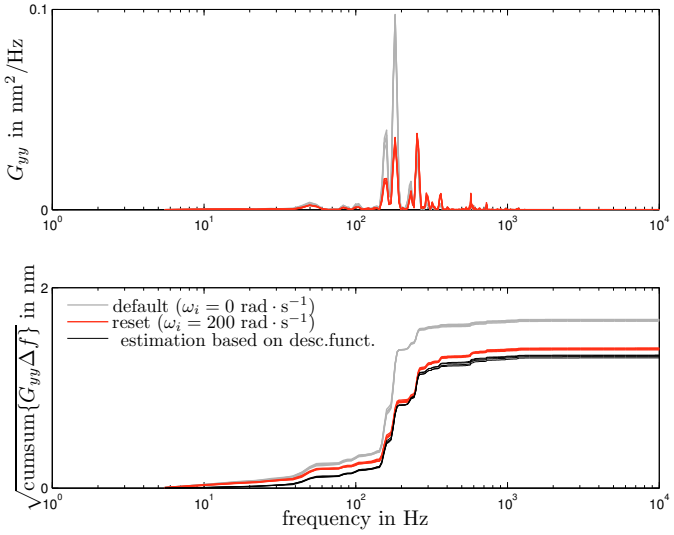

Fig. 9. Time series measurement; power spectral density analysis (upper part) of four responses to the same commanded reference either with (red) or without (grey) extra reset integrator along with a cumulative root-mean-square representation (lower part).

seen that the reset control design (red) has reduced low-frequency content with respect to the default control design (grey) without significant high-frequency deterioration. Based on the measured power spectral densities of the default control design (grey curves in Fig. 9) and the respective sensitivities of the default design and the reset control design (grey and red curves in Fig. 7), the power spectral densities of the reset control design can also be estimated, see the black curves in Fig. 9. The estimates seem to provide fair lower bounds on the measured power spectral densities (red curves), which can (partly) be explained by the fact that higher-order harmonics are neglected in the describing function analysis.

4. CONCLUSION

Reset integral control has been demonstrated to enhance the performance of an industrial wafer stage system. Moreover, sufficient conditions, that can be checked by measured frequency-response functions, have been given that render the closed-loop system stable. Less conservative stability conditions and tighter frequency-domain based performance estimates are expected to enhance the reset control design even further and remain topics of interest.

REFERENCES

W.H.T.M. Aangenent, G. Witvoet, W.P.M.H. Heemels, M.J.G. Van De Molengraft, and M. Steinbuch. (2010) Performance analysis of reset control systems, Int. J. of Robust and Nonlinear Control, 20(11), pp.1213-1233.

M. Arcak, M. Larsen, and P. Kokotovic. (2003) Circle and Popov criteria as tools for nonlinear feedback design, Automatica, 39(4), pp. 643-650.

A. Baños, J. Carrasco, and A Barreiro. (2011) Reset times-dependent stability of reset control systems, IEEE Trans. on Automatic Control, 56(1), pp. 217-223.

O. Beker, C.V. Hollot, Y. Chait, and H. Han. (2004) Fundamental properties of reset control systems, Automatica, 40(6), pp. 905-915.

H. Butler. (2011) Position control in lithographic equipment; an enabler for current-day chip manufacturing. Control Systems Magazine, 11, pp. 28-47.

J. Carrasco, A. Baños, and A. van der Schaft. (2010) A passivity-based approach to reset control systems stability, System & Control Letters, 59(1), pp. 18-24.

J.C. Clegg. (1958) A nonlinear integrator for servomechanisms, Trans. AIEE, 77(1), pp. 41-42.

F. Forni, D. Nešić, and L. Zaccarian. (2011) Reset passivation of nonlinear controllers via a suitable time-regular reset map, Automatica, 47(9), pp. 2099-2106.

K.G.J. Gruntjens, M.F. Heertjes, S.J.L.M. van Loon, N. van de Wouw, and W.P.M.H. Heemels. (2016) Switching Integral Reset Control: Application to a Lens Motion System, In preparation.

M.F. Heertjes, K.G.J. Gruntjens, S.J.L.M. van Loon, N. Kontaras, and W.P.M.H. Heemels. (2015) Design of a Variable Gain Integrator with Reset, In Proc. of the American Control Conference, Chicago, Illinois, USA, pp. 2155-2160.

S.J.L.M. van Loon, K.G.J. Gruntjens, M.F. Heertjes, N. van de Wouw, and W.P.M.H. Heemels. (2016) Frequency-domain tools for stability analysis of reset control systems, Submitted to Automatica.

I. Horowitz, and P. Rosenbaum. (1975) Non-linear design for cost of feedback reduction in systems with large parameter uncertainty, Int. J. of Control, 21(6), pp. 977-1001.

D. Nešić, L. Zaccarian, and A.R. Teel. (2008) Stability properties of reset systems, Automatica, 44(8), pp. 2019-2026.

M.M. Seron, and G.C. Goodwin. (1996) Sensitivity limitations in nonlinear feedback control, Systems & Control Letters, 27, pp. 249-254.

L. Zaccarian, D. Nešić, and A.R. Teel. (2005) First order reset elements and the Clegg integrator revisited, American Control Conference (ACC 2005), 1, pp. 563-568.

L. Zaccarian, D. Nešić, and A.R. Teel. (2010) Analytical and numerical Lyapunov functions for SISO linear control systems with first-order reset elements, Int. J. of Robust & Nonlinear Control, 21(10), pp. 1134-1158.